JOURNAL OF THERMOPHYSICS AND HEAT TRANSFER
Vol. 19, No. 2, April–June 2005

Transition in Low-Pressure Turbines: Effects of Unsteady Acceleration and Turbulence Intensity

Nan Jiang* and Terrence W. Simon†
University of Minnesota, Minneapolis, Minnesota 55455

Wakes generated by upstream airfoil rows create an unsteady flowfield to downstream rows of a low-pressure turbine. Pressure gradients and local turbulence intensity levels imposed on the airfoil surface boundary layers change as the wakes pass through the passage. Separation and laminar-to-turbulent transition onset locations and transition path characteristics also change during the wake passing cycle. The effects of unsteady acceleration (composed of spatial acceleration and temporal acceleration) and time variations in turbulence intensity on transition onset and transition path are described. Results come from an experiment in which the wakes and passage flow of a low-pressure turbine are simulated. The total acceleration field is separated into spatial and temporal components. Also important is the changing turbulence field as affected by passing wakes. Deceleration and high turbulence levels, as experienced by the boundary layer as the wake approaches, promote transition, whereas acceleration and low levels of turbulence, experienced as the wake departs, can delay transition.

Nomenclature

L	=	chord length
L_{ss}	=	suction surface length
L_z	=	span
Re	=	Reynolds number
$Re_{L_{ss}}$	=	Reynolds number based on the suction surface length and exit velocity
P	=	pitch
s	=	distance along the blade's suction surface from the leading edge stagnation line
TI	=	local turbulence intensity $\tilde{u}_{rms}/\tilde{u}$
$\tilde{T}I$	=	ensemble-averaged turbulence intensity
U	=	freestream velocity at the separation point
U_a	=	approach flow velocity
U_{local}	=	local velocity at the edge of the boundary layer
U_{rms}	=	rms fluctuation of U_{local}
u_r	=	wake generator velocity (rod velocity)
u_x	=	axial component of inlet velocity
$\tilde{u}$	=	ensemble-averaged velocity
$\tilde{u}_{rms}$	=	ensemble-averaged velocity fluctuation
x	=	normalized position along the suction surface s/L_{ss}, %
x_s	=	x at the separation point
x_t	=	x at transition onset point
y	=	distance normal to the wall
β_1	=	blade inlet angle
β_2	=	blade outlet angle
γ	=	intermittency (fraction of the time the flow is turbulent or fraction of the surface covered by turbulent flow)
$\tilde{\gamma}$	=	ensemble-averaged intermittency
θ	=	phase angle within the wake passing period or momentum thickness, depending on context
λ_θ	=	pressure gradient parameter

Presented as Paper 2003-3630 at the AIAA 36th Thermophysics Conference, Orlando, FL, 23–26 June 2003; received 8 April 2004; revision received 9 August 2004; accepted for publication 10 August 2004.

*Research Assistant, Ph.D. Candidate, Heat Transfer Laboratory, Department of Mechanical Engineering, 111 Church Street Southeast. Student Member AIAA.

†Professor, Heat Transfer Laboratory, Department of Mechanical Engineering, 111 Church Street Southeast. Member AIAA.

Introduction

STREAMWISE pressure gradients and freestream turbulence intensity are known to influence transition onset and the transition path. Gostelow et al.[1] compared measurements of boundary-layer transition under six different turbulence levels and a wide range of adverse pressure gradients. The transition length became severely reduced as the strength of the adverse pressure gradient increased. Consistent with this, the turbulent spot formation rate was found to increase. Solomon et al.[2] found that transition in regions of strongly changing pressure gradient showed quite different characteristics than those predicted by correlations of data from flows in which the pressure gradient parameter remained uniform throughout the transition zone. Using the local pressure gradient was shown to be moderately successful in the prediction of transition in such flows. Simon et al.[3] showed how high freestream turbulence intensity causes a more upstream transition. Volino[4,5] measured separated-flow transition under low-pressure turbine (LPT) conditions. Cases varied in Reynolds number and freestream turbulence intensity. Results were discussed in terms of mean and fluctuating velocity profiles, turbulent shear stress profiles, and intermittency profiles. From power spectral distributions, transition was identified by the emergence of a sharp peak in the spectra when the freestream turbulence level was low and a growth of broadband turbulence when the freestream turbulence level was elevated. The latter is a characteristic of strong bypass transition.[6] Volino et al.[7] applied conditional sampling against data from a transitional boundary layer subject to high (initially 9%) freestream turbulence intensity and strong acceleration to separate the turbulent and nonturbulent zone data. Eddy transport in the nonturbulent zone was significant, however, and the nonturbulent zone did not behave precisely like a laminar boundary layer. The marked difference between transport levels in laminar vs turbulent flow indicated a distinct need for accurate transition modeling and proper handling of the effects of freestream turbulence and streamwise acceleration on the pretransitional flow.

In turbomachinery, the passing wakes from the upstream airfoils cause the flow to be unsteady. In particular, pressure gradients and turbulence intensity levels change throughout the wake passing cycle. Lou and Hourmouziadis[8] experimentally studied separation and laminar-to-turbulent transition on a plate under the influence of unsteady pressure gradients. The periodic-unsteady main flow was found to induce an oscillation of the separation bubble. Transition

and the associated reattachment of the separation bubble were dominated by the free shear layer instability. Wolff et al.[9] investigated unsteady, wake-affected transition of a boundary layer on a linear LPT cascade suction surface. Between the passing wakes, quasi-steady flow conditions were reestablished. Kaszeta,[10] Kaszeta and Simon,[11] and Kaszeta et al.[12,13] simulated an LPT flow passage, including the effects of passing wakes, and then documented the unsteady flowfield over the suction surface. The Kaszeta data set[10] is used in the present paper. Yaras[14] suggested that separation-bubble transition depends on the pressure gradient history of the laminar boundary layer before the separation. Howell et al.[15] measured unsteady boundary-layer behavior in two, high-lift geometries and one, ultra-high-lift LPT geometry using surface-mounted hot-film sensors. Regions of wake-induced transition, natural transition, and calming in the boundary layer were identified, and effects of passing wakes on these regions were discussed. The calmed boundary layer is that which follows, and is thinned (stabilized) by, the turbulent spot.

The velocity deficit within a passing wake in a turbomachinery flow causes the freestream velocity over the suction surface boundary layer to oscillate during the wake passing cycle. This oscillation causes a temporal acceleration and deceleration of the flow, $\partial u/\partial t$. Also, the freestream velocity changes spatially along the suction surface due to the passage geometry, $u(\partial u/\partial s)$. This spatial acceleration also changes throughout the wake passing cycle by virtue of the velocity change associated with the passing wake. The total acceleration or substantial derivative of the velocity is the sum of temporal and spatial acceleration components,

$$\frac{\mathrm{D}u}{\mathrm{D}t} = \frac{\partial u}{\partial t} + u\frac{\partial u}{\partial s}$$

In this paper, we will describe these acceleration components measured within an experiment that simulates LPT flow conditions. We will discuss the effects they have on transition onset and on the transition path. Kaszeta,[10] Kaszeta and Simon,[11] and Kaszeta et al.[12,13] documented the ensemble-averaged distributions of velocity $\tilde{u}(s, y, \theta)$, rms fluctuation of velocity $\tilde{u}_{\mathrm{rms}}(s, y, \theta)$, local turbulence intensity $\tilde{T}\,I(s, y, \theta)$, and fraction of the time the flow is turbulent and the intermittency $\tilde{\gamma}(s, y, \theta)$, for a simulation of a LPT suction surface flow under very low Reynolds number ($Re_{L_{\mathrm{ss}}} = 5 \times 10^4$) conditions. They used an ensemble size of 100 wake passing cycles for their averaging. With these data, we can calculate the ensemble-averaged spatial acceleration, temporal acceleration, and total acceleration of the wake passing cycle. We then discuss the relationship between the acceleration and transition characteristics.

Experiment

Experimental Facility

The experimental facility consists of a low-speed wind tunnel, a wake generator, and a turbine cascade simulator. Each will be discussed.

Low-Speed Wind Tunnel

All experiments were done using a low-speed, open-return, blown-type wind tunnel (Fig. 1). This facility consists of a filter box, a blower, a redistribution section, an oblique header, a heat exchanger, a flow conditioning section, a nozzle, a developing section, and the test section. The flow is delivered to the developing section uniformly and steadily in velocity and temperature and at a low turbulence intensity (~0.5%).

Turbulence Generation

A turbulence generator grid (Fig. 2) raises this approach flow turbulence level to 2.5%. This grid is located in the developing section 45.5 cm downstream of the nozzle exit and about 100 cm upstream of the inlet plane shown in Fig. 3. It consists of nine rods that are evenly spaced in the horizontal (cross-stream) direction and two rods arranged in the vertical (spanwise) direction, as shown.

Wake Generator

The wake generator (Fig. 3) installed in the developing section simulates wakes emerging from upstream turbine rows in an LPT. It consists of a moving sled assembly containing the wake generating objects (0.635-cm-diam stainless steel rods), an H-beam rail upon which the sled slides, a speed-controlled motor and transmission assembly to drive the sled, and a dashpot to stop it. The rods are driven at a uniform speed until the end of the traverse; then they are returned for the next traverse. Data from four of seven rods on the sled are used for processing. Measurements indicated that their wakes are similar to one another, whereas the wakes from the first two rods and the last rod are slightly different. Details can be found by Kaszeta,[10] Kaszeta and Simon,[11] and Yuan.[16]

Test Surface

The airfoil surface geometry (Fig. 4 and Table 1) is the PAK-B airfoil shape offered for research by Pratt and Whitney and used in numerous studies.[3–5,7,10–13,17–21] Coordinates of this airfoil, which has become a standard test airfoil for LPT transition studies, may be found in the literature, for example, Refs. 3 and 11. Measurements used in this study were taken at the midspan of the test section, which has an aspect ratio of 6. Access is provided through the pressure surface wall, as needed. Wall-normal profiles were collected at 10 streamwise locations along the suction surface, stations P04–P13, at 30 different wall-normal distances ranging from $y = 0.1$ mm to $y = 16.5$ mm, unevenly spaced with steps ranging from $\Delta y = 0.1$ mm near the wall to $\Delta y = 1$ mm approaching the freestream. (See Table 2 for measurement locations.)

The single-sensor anemometry is used in this study to obtain instantaneous time-series measurements of velocity and velocity fluctuations. The overall uncertainty of the velocity and turbulence intensity measurements is 5%, based on a 95% confidence interval.

Base Case

The test facility is designed to produce flow conditions that simulate an LPT environment. All measurements used herein are with $Re_{L_{\mathrm{ss}}} = 5 \times 10^4$ and approach flow turbulence intensity (AFTI, defined as $U_{a,\mathrm{rms}}/U_a$) = 2.5%. The steady-state experimental results (no wakes) discussed by Simon et al.[3] and Qiu[18] showed laminar flow separation followed by transition of the separated shear layer and reattachment near the trailing edge, leading to a large separation bubble for this case. The pressure distribution for this case is shown in Fig. 5 along with the high Reynolds number design distribution of this PAK-B airfoil. A similar case, but with AFTI = 10%, showed

Table 1 PAK-B airfoil details

Parameter	Value
Chord length L, mm	114
Pitch P, mm	91.2
Span L_Z, mm	684
Blade inlet angle β_1, deg	35
Blade outlet angle β_2, deg	−60
Flow coefficient u_x/u_r	1.43

Table 2 Pressure taps and profile locations (same) on the suction surface

Tap	s/L_{ss}, %
P01	0.00
P02	5.19
P03	19.78
P04	31.36
P05	37.35
P06	43.34
P07	49.33
P08	55.33
P09	61.32
P10	70.31
P11	76.11
P12	84.00
P13	93.49

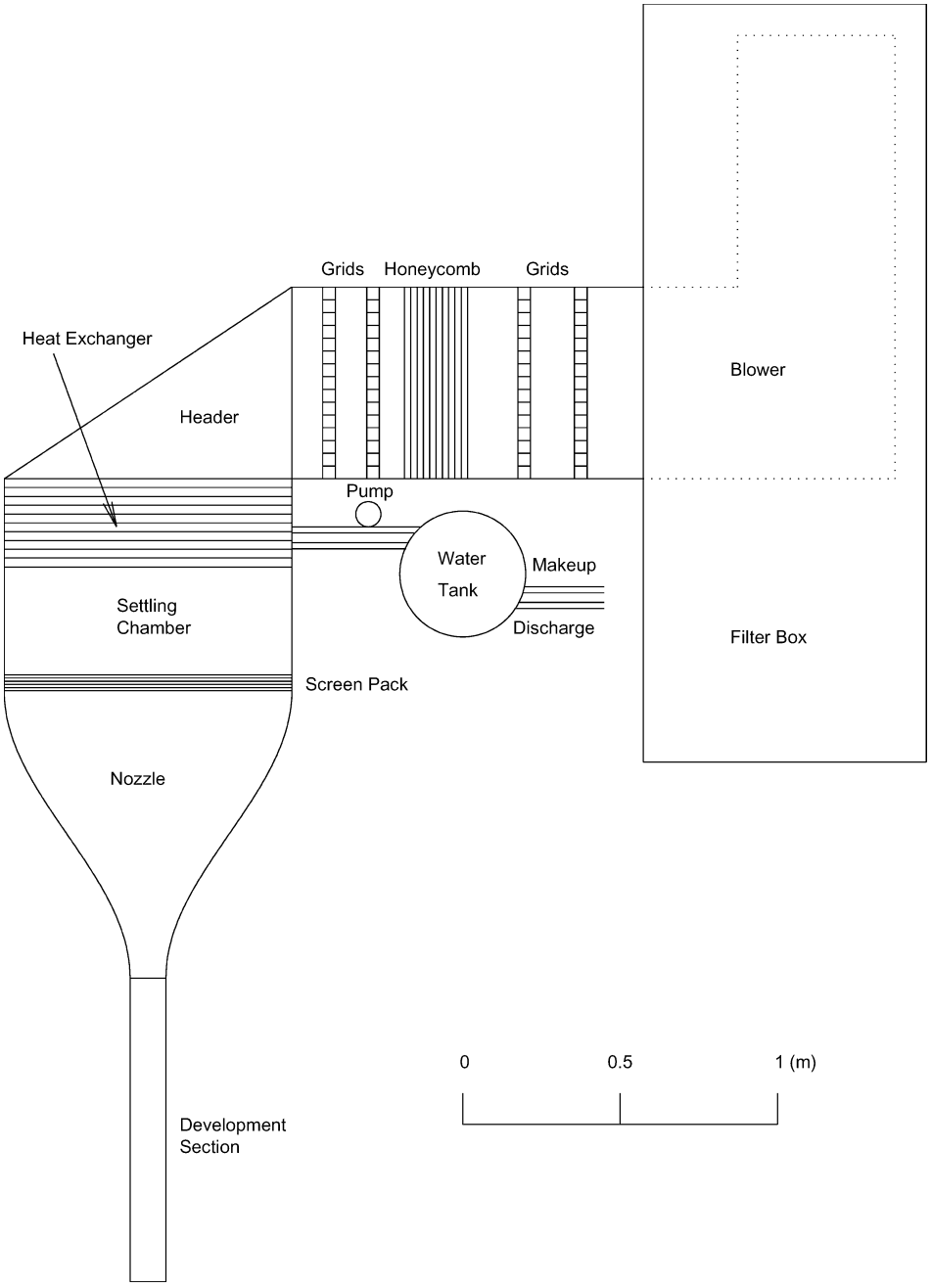

Fig. 1 Schematic of experimental facility.

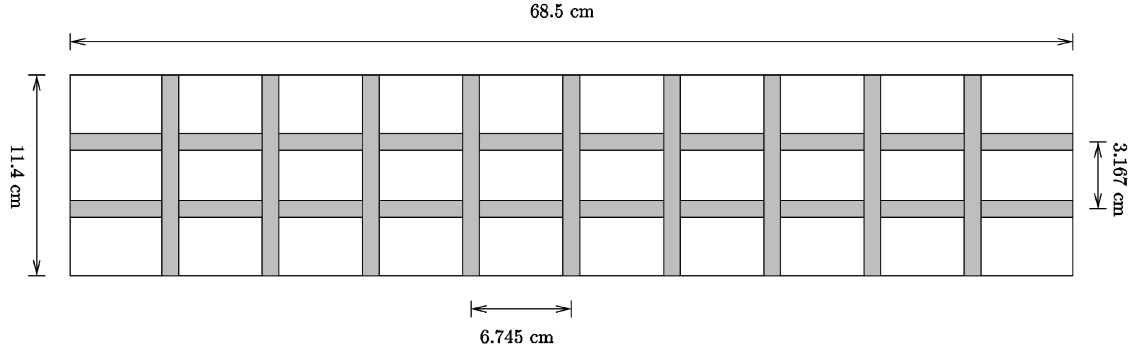

Fig. 2 Rod-grid turbulence generator used for $TI = 2.5\%$; each rod is 0.95 cm in diameter.

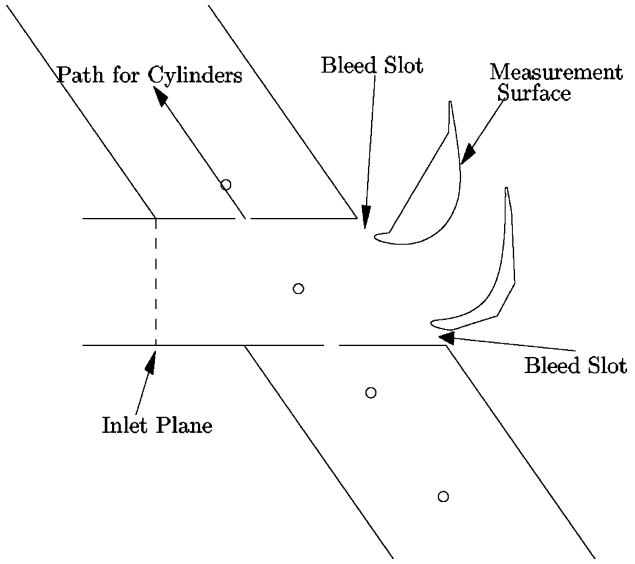

Fig. 3 Cross-sectional view of the experimental facility.

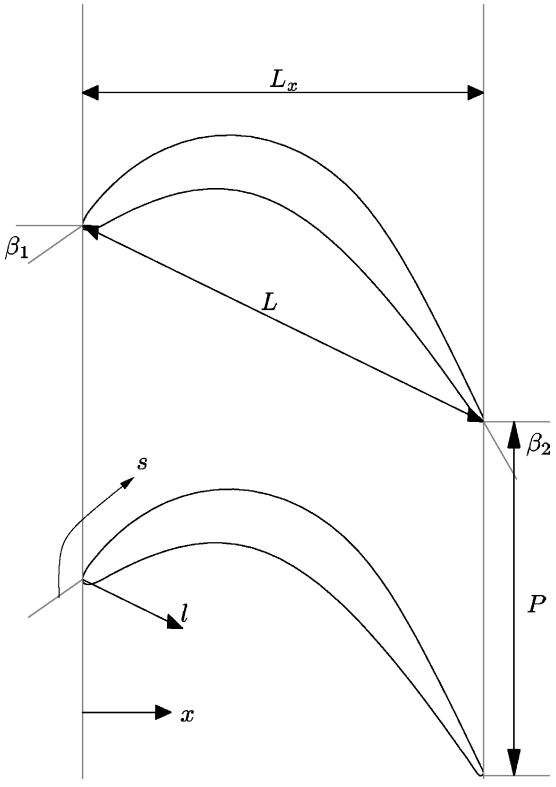

Fig. 4 Important flow and geometry characteristics; parameter values in Table 1.

separation, transition of the separated shear layer, and reattachment, with a very small separation bubble. This second case is noteworthy because the peak turbulence within the wakes of the present case is approximately 10%. The pressure profile for the steady flow (no-wake) AFTI = 10% case is shown also in Fig. 5.

The case discussed in this paper has wakes. The inlet velocity $u_x = 3.03$ m/s, and the wake generator velocity $u_r = 0.7u_x$, or 2.12 m/s. The wake passing frequency is 23.2 Hz. For this case, ensemble-averaged distributions of $\tilde{u}(s, y, \theta)$, $\tilde{u}_{\text{rms}}(s, y, \theta)$, $\tilde{T}I(s, y, \theta)$, and $\tilde{\gamma}(s, y, \theta)$ were recorded for each of 12 stations spaced along the suction surface length.

The raw velocity signals were processed using the turbulent event recognition algorithm (TERA) of Falco and Gendrich,[22] as modified by Walker and Solomon,[23] to obtain the turbulence intermittency function. This function has two states, 0 or 1, to indicate whether the flow is laminar or turbulent, respectively. The intermittency value $\tilde{\gamma}$ is the phase-averaged value of the intermittency function. A more complete discussion of the TERA algorithm used in this study may be found by Kaszeta and Simon.[11] The profiles of near-wall intermittency in the attached flow or intermittency over a separation bubble are used to determine transition onset. We look for a sharp and sustained rise in intermittency to indicate that transition has begun. This process requires some effort. The entire data set (time and space variations) must be reviewed to determine the onset of transition. For θ values during which the flow is separated, we note that this is at the edge of the separation zone as indicated by the mean velocity and turbulence level plots. The transition onset location is given with an estimated uncertainty of 5% in s/L_{ss}. We found that movies showing the time-varying data were far more valuable than still photographs for this process.

A sheet of hot-film surface sensors (Senflex Systems sensor sheet Model SF9501) was used to identify the unsteady separation points. The thin-film sensors were powered by a hot-wire anemometer bridge. The voltage required to maintain the sensor at the desired temperature is related to the wall shear stress at that sensor.[24] Because it was only related to the shear stress and not directly correlated with the shear stress, the term applied is pseudoshear stress. The skewness distribution of the pseudoshear stress was monitored as one indicator of incipient separation because it was determined[25] that a sudden drop of skewness indicates incipient separation. Used also in determining the unsteady separation location were the velocity and turbulence intensity field data.

Uncertainty Analysis

The uncertainties in the calculation accelerations are difficult to assign. We can measure our velocity to within 5% of these data over most of the flowfield. Our temporal resolution is 1/90 of a cycle and our spatial resolution in the streamwise direction is approximately 7–8% of L_{ss}. Thus, we estimate uncertainties of $\partial u/\partial t$ and $\partial u/\partial s$ of 10 and 17%, respectively.

Unsteadiness due to Passing Wakes

The wakes periodically pass through the turbine blade passage. This causes the total flowfield to be unsteady. The pressure gradient field, the local turbulence intensity field, and the convection field are all changing during the wake passing period. In this section, we will discuss this unsteadiness. The following discussion is guided by visualizing movies of the $\tilde{u}$, $\tilde{u}_{\text{rms}}$, $\tilde{T}I$ and $\tilde{\gamma}$ data (essentially, dynamic pictures of Fig. 6 changing with θ, the angular position within the 360-deg wake passing period).

Figures 6a, 6b, and 6f show profiles of velocity, turbulence intensity and intermittency at $\theta = 292$ deg. High intermittency is seen in the freestream within the passing wake (centered at $s/L_{\text{ss}} = 70\%$ at this time) due to elevated turbulence and high advection velocity. The algorithm used to compute intermittency shows high values for a combination of high frequency and high disturbance level. The movement of the passing wakes can be viewed as the moving region of high intermittency in the core flow. The velocity deficit of the moving wake will make the main flow velocity oscillate. A temporal acceleration is caused, and spatial acceleration is made unsteady, by this oscillation. Generally, as the wake arrives, there is a local and instantaneous deceleration followed by an acceleration. The deceleration leads the wake by about 10–20% of the suction surface length and the acceleration lags the wake by about 10–15% of the suction surface length. Figure 6 shows this in the velocity (Fig. 6a) and the total acceleration (Fig. 6c). Note that at this position within the cycle ($\theta = 292$ deg), the deceleration is centered at $s/L_{\text{ss}} = 80$–90% and the acceleration is centered at 40–60%.

The spatial acceleration profile (Fig. 6e) is mainly influenced by the passage geometry, but it is also affected by the passing wake. The presence of the wake will cause a local decrease in the flow velocity as it approaches. Downstream, the flow recovers. Therefore, local spatial acceleration precedes the wake arrival time. This spatial acceleration and deceleration will vary with streamwise location. At

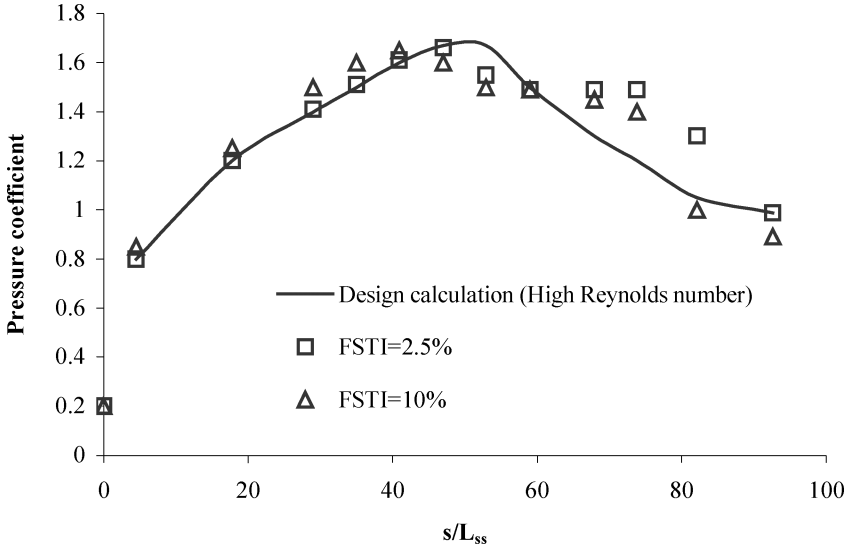

Fig. 5 Pressure distribution on the suction surface of PAK-B airfoil.

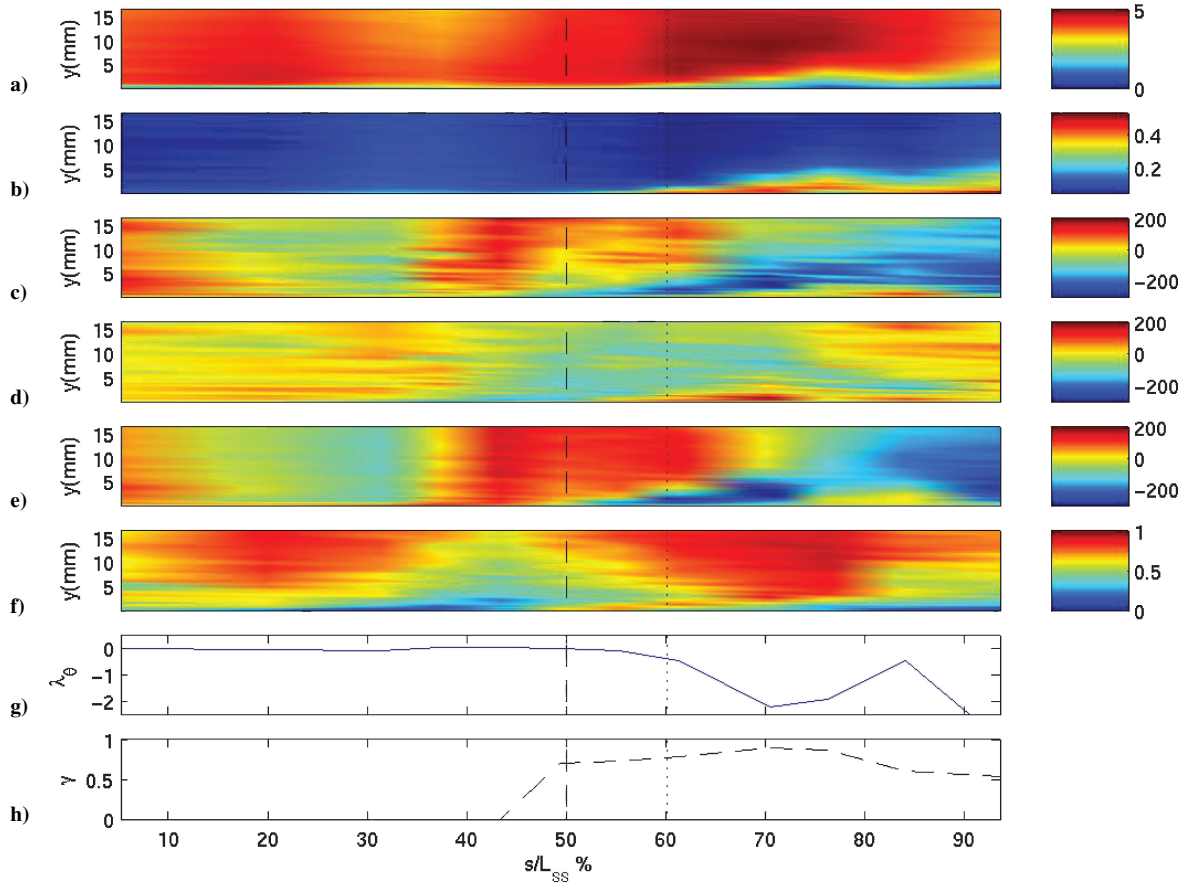

Fig. 6 At $\theta = 292$ deg, profiles of a) velocity, m/s b) turbulence intensity $\tilde{TI}$, c) total acceleration, m/s^2, d) temporal acceleration, m/s^2, e) spatial acceleration, m/s^2, f) intermittency, g) pressure gradient parameter, and h) peak intermittency in the boundary layer: – – –, transition onset and . . . . , separation.

the throat of the passage (about $s/L_{ss} = 45\%$), the flow experiences higher velocities. Thus, generally, there is acceleration ahead of the throat and deceleration downstream. At the trailing edge of the blade, the suction surface flow generally experiences deceleration, except near the wall, where transition, if it is present, is accelerating the flow due to improved mixing with the main stream. Generally the largest deceleration is near the wall immediately downstream of the throat. This is due mostly to the passage geometry. As expected, this deceleration has a dominant effect on boundary-layer stability, separation, and transition.

The total derivative is the sum of the temporal acceleration and the spatial acceleration. We find that total acceleration (Fig. 6c) has more of the characteristics of spatial acceleration, $u(\partial u/\partial s)$ (Fig. 6e) than those of temporal acceleration, $\partial u/\partial t$ (Fig. 6d). As the flow approaches the throat region of the passage, it accelerates, whereas over the downstream portion of the blade, there is deceleration. There is also a strong deceleration region near the wall immediately downstream of the throat of the passage. It is in this region that boundary-layer separation is observed. For the case discussed, separation is observed during most of the cycle. Note that, generally,

much of the far-field flow is decelerating at this location. However, because of the passing wake, this deceleration region changes. When the wake is approaching, the level of deceleration in this region is the largest. Just after the wake passes, the level of deceleration is the weakest. Thus, the size and location of this decelerating flow region change as the wake passes.

Oscillation of the freestream due to passing wakes is visible in the velocity traces. The boundary layer is particularly influenced by the passing wakes. We see that the boundary layer thickens more rapidly in the region $60 < s/L_{ss} < 70\%$. This is where separation is observed, as indicated by a near-zero, near-wall velocity. The separation point changes throughout the wake passing cycle. When the freestream is accelerating at a particular streamwise location, the boundary layer at that location will thin. If the freestream accelerates where the boundary layer tends to separate, the flow will recover and separation will be delayed.

Also, the turbulence intensity is affected by the passing wake. When the wake comes, the turbulence intensity at the inlet of the passage will increase. The turbulence intensity of the freestream increases as the wake moves along the surface. After the wake passes, the freestream turbulence intensity recovers to the between-wake levels.

Effects of Unsteady Turbulence Intensity and Acceleration

Transition Onset

Because of the unsteadiness of the turbulence intensity and acceleration, transition onset, as described by the near-wall intermittency distribution (Fig. 6f) in the transition region, will change. During the wake passing cycle, two modes of transition, attached flow transition and separated flow transition, are found. Both the transition onset location x_t and the flow separation location x_s move forward and rearward during the wake passing cycle (Fig. 7). The transition path from laminar to turbulent flow is obviously affected by the passing wake. This can be observed in the near-wall intermittency (Fig. 6f or 6h).

In the period $224 < \theta < 312$ deg, attached-flow transition is found in the region near the passage throat, $s/L_{ss} = 45\%$. It moves toward the trailing edge as time passes. At $\theta = 292$ deg (Fig. 6), separation is observed at $s/L_{ss} = 60\%$ (dotted line in Fig. 6), whereas transition onset (dashed line in Fig. 6) is at $s/L_{ss} = 50\%$. The boundary layer thickens after the separation point; see near-wall velocities in Fig. 6a. At this time, the wake had just passed this region (Fig. 6f). Recall that the high intermittency in the freestream marks the wake. In the boundary layer, high intermittency shows transition. The flow is decelerating temporally (Fig. 6d) in the freestream in this region at the time shown in Fig. 6, whereas there is a small part near the wall where the flow is beginning to accelerate. Spatial acceleration (Fig. 6e) in the freestream in this region is strong due to its nearness to the passage throat. However, immediately downstream of the throat, there is a decelerating region near the wall. These two regions are both affected by the passing wake. The sum of the spatial acceleration and the temporal acceleration, total acceleration, is shown in Fig. 6c. The total acceleration distribution looks more like the spatial acceleration distribution than the temporal acceleration distribution, although the levels of acceleration and deceleration are different. Comparing Fig. 6c with Fig. 6f, we can find a strong correlation between total acceleration and transition, as expected. Transition onset is in the deceleration region. Figure 6g shows a profile of the pressure gradient parameter, $\lambda_\theta = (\theta^2/\nu)(\partial U_{local}/\partial s)$. The trend of this parameter agrees with the spatial acceleration or total acceleration trend. It is weak until $s/L_{ss} = 50\%$, but shows an obvious decrease in value thereafter. When the flow is accelerating, the boundary layer remains thin. In the boundary layer beneath the wake, the turbulence intensity is high (Fig. 6b). The high unsteadiness in the wake destabilizes the flow. It is another trigger to the onset of transition. The distribution of the peak intermittency in the boundary layer (Fig. 6h) will be discussed in the next section.

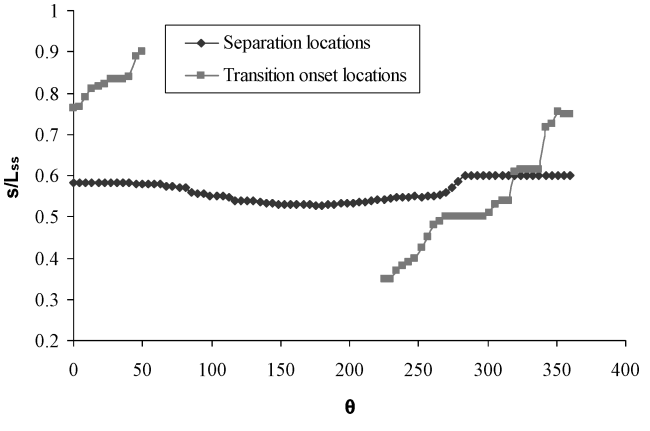

Fig. 7 Separation and transition location during cycle.[10]

At $\theta = 0$ deg (the time chosen for Fig. 8), the separation point is at $s/L_{ss} = 58\%$. In this period, the wake has moved far downstream of the passage throat and is near the trailing edge. From the velocity profile (Fig. 8a), we can see the boundary layer begins to thicken at this point. Transition starts at $s/L_{ss} = 76\%$, as indicated by the elevated level of intermittency near the wall (Fig. 8f). In the freestream, the intermittency at the trailing edge is large, indicating the presence of the wake. From the passage throat to the trailing edge, the flow is temporally decelerating (Fig. 8d) except for a small portion of acceleration near the wall at the trailing edge. The flow at the trailing edge is decelerating spatially (Fig. 8e). The total effect of the temporal deceleration and the spatial deceleration is the strong total deceleration shown in Fig. 8c. The profile of the pressure gradient parameter λ_θ shows a strong deceleration at the location of transition onset (Fig. 8g). The turbulence intensity in the boundary layer downstream of transition is large, reaching its peak at the streamwise position of the wake.

In the period $56 < \theta < 220$ deg, no transition can be seen. Figure 9 shows the flow status at $\theta = 136$ deg. Separation is at $s/L_{ss} = 54\%$ (Fig. 9a). The wake is entering the passage at the leading edge, $s/L_{ss} = 10\%$ (Fig. 9f). In the region from the passage throat to the trailing edge, the intermittency value is small, indicating that the flow is stable in this region. No sign of transition is indicated. The flow near the throat is temporally accelerating (Fig. 9d). The profiles of total acceleration and spatial acceleration in this period are not very different from those taken during a period in which transition is observed, such as $\theta = 292$ deg. (Compare Figs. 9c and 6c and Figs. 9e and 6e.) The only difference is that the wake is not in the deceleration region of flow ($s/L_{ss} > 40\%$). Thus, we can conclude that destabilization by the wake is important to transition onset. We notice that transition will always take place in a flow deceleration region. Note also that turbulence intensity in the boundary layer upstream of the throat does not change in a spatial sense regardless of the position of the wake (Fig. 9b).

Transition Path

In the steady case (the no-wake case discussed by Qiu and Simon[19]), transition proceeds until the flow is fully turbulent. However, in the unsteady case the situation changes. The unsteady pressure gradients affected by the passing wake may cause temporal acceleration while the flow is decelerating spatially. Such a situation may retard the transition process. For instance, at $\theta = 292$ deg (Figs. 6h and 6f), transition onset is at $s/L_{ss} = 50\%$. Because of destabilization as a result of the wake being present, transition develops quickly at the beginning (Fig. 6h). However, we see its progress slow, and then we see a decrease in intermittency downstream of $s/L_{ss} = 75\%$ (Fig. 6h). From Fig. 6g, we see that the deceleration level begins to decrease at this location, and we see that the flow is temporally accelerating at this location (Fig. 6d). Thus, the streamwise progression of transition is retarded. This is characteristic of the period $224 < \theta < 312$ deg. Typically, transition-path modeling, extended from the works of Emmons,[26] assumes that transition proceeds in the streamwise direction with ever-increasing intermittency values. These data indicate that unsteady-flow transition modeling must include this stabilization effect.

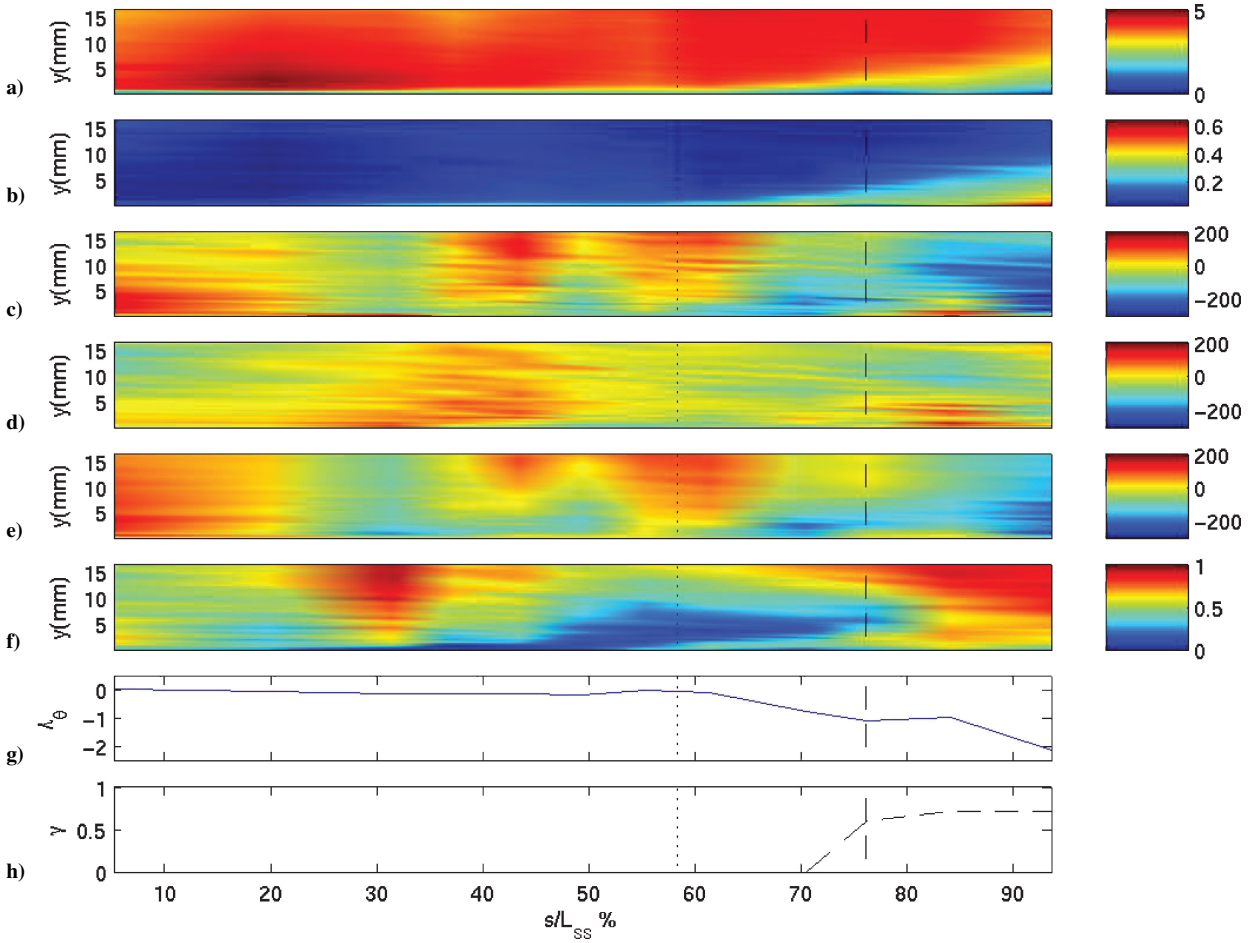

Fig. 8 At $\theta = 0$ deg, profiles of a) velocity, m/s, b) turbulence intensity $\tilde{T}I$, c) total acceleration, m/s^2, d) temporal acceleration, m/s^2, e) spatial acceleration, m/s^2, f) intermittency, g) pressure gradient parameter, and h) intermittency in boundary layer.

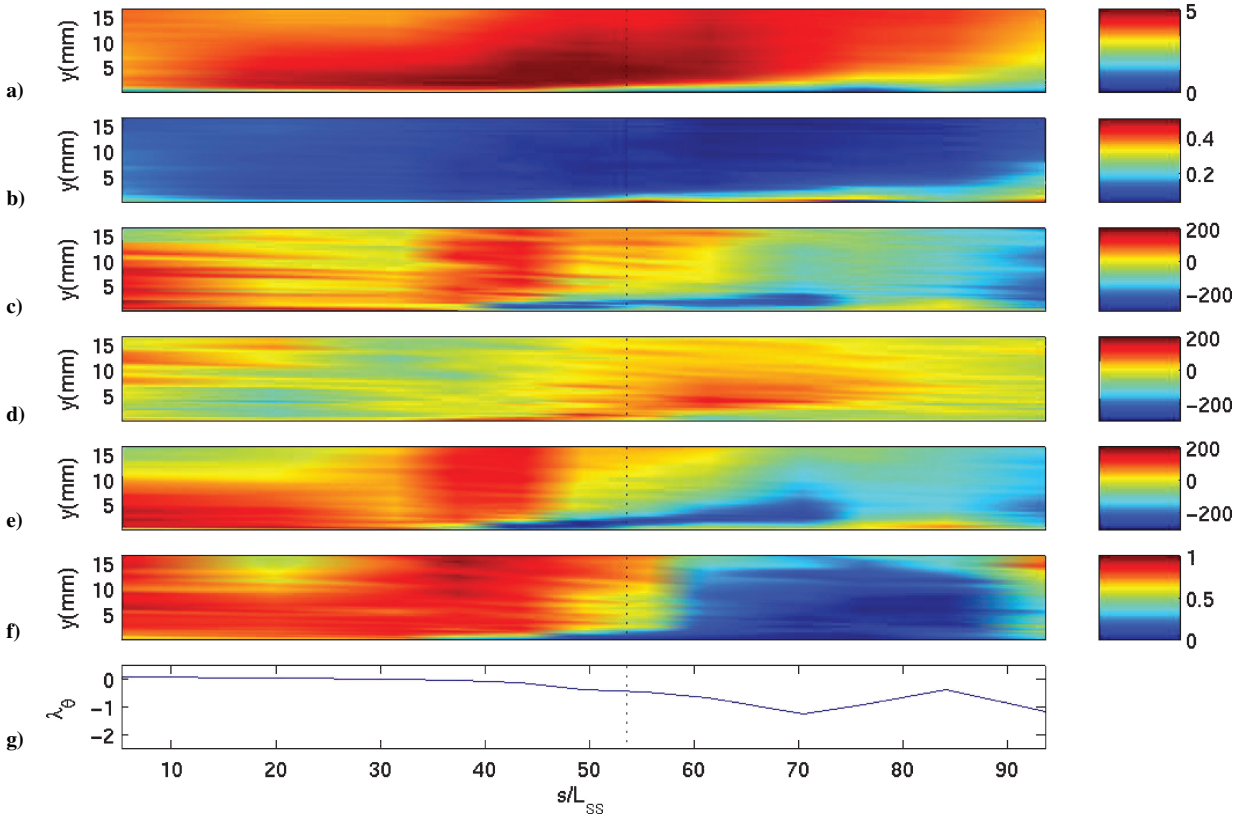

Fig. 9 At $\theta = 136$ deg, profiles of a) velocity, m/s, b) turbulence intensity $\tilde{T}I$, c) total acceleration, m/s^2, d) temporal acceleration, m/s^2, e) spatial acceleration, m/s^2, f) intermittency, and g) pressure gradient parameter.

In the periods $0 < \theta < 50$ deg and $320 < \theta < 360$ deg, transition is not retarded as discussed earlier. In these periods, the wake is moving within the decelerating flow region near the trailing edge and in the freestream there is no temporal acceleration.

The application of transition-path models to the data set discussed herein was presented by Jiang and Simon.[20,21]

Summary

The unsteadiness caused by the passing wake substantially changes the transition situation within the LPT passage. Though the flow responds to total acceleration, it is instructive to consider temporal acceleration and spatial acceleration separately in discussing modeling of transition onset. The transition onset location is not fixed in time or space, but is moving on the suction surface in an unsteady fashion. Turbulence within the wake is also important. In this study, we document the effects that wake-associated acceleration and wake-associated turbulence have on the flow. We see transition onset either upstream or downstream of separation, periods of complete transition to turbulence, extended (spatially) transition zones, and streamwise decreasing intermittency indicating a streamwise reversal of the transition process. Clearly, transition models that capture the entire unsteady transition process of the LPT must be capable of capturing all of these features.

Acknowledgments

The University of Minnesota transition work is part of a study of transition in low-pressure turbines sponsored by NASA John H. Glenn Research Center under Cooperative Agreement NCC3-652. The contract monitor is David Ashpis.

References

[1]Gostelow, J. P., Blunden, A. R., and Walker, G. J., "Effects of Free-Stream Turbulence and Adverse Pressure Gradients on Boundary Layer Transition," *Journal of Turbomachinery*, Vol. 116, No. 3, 1994, pp. 392–404.

[2]Solomon, W. J., Walker, G. J., and Gostelow, J. P., "Transition Length Prediction for Flows with Rapidly Changing Pressure Gradients," *Journal of Turbomachinery*, Vol. 118, No. 4, 1996, pp. 744–751.

[3]Simon, T. W., Qiu, S., and Yuan, K., "Measurements in a Transitional Boundary Layer Under Low-Pressure Turbine Airfoil Conditions," NASA CR-209957, March 2000.

[4]Volino, R. J., "Separated Flow Transition Under Simulated Low-Pressure Turbine Airfoil Conditions: Part 1—Mean Flow and Turbulence Statistics," *Journal of Turbomachinery*, Vol. 124, No. 4, 2002, pp. 645–655.

[5]Volino, R. J., "Separated Flow Transition Under Simulated Low-Pressure Turbine Airfoil Conditions: Part 2—Turbulence Spectra," *Journal of Turbomachinery*, Vol. 124, No. 4, 2002, pp. 656–664.

[6]Mayle, R. E., Dullenkopf, K., and Schulz, A., "The Turbulence that Matters," *Journal of Turbomachinery*, Vol. 120, No. 3, 1998, pp. 402–409.

[7]Volino, R. J., Schultz, M. P., and Pratt, C. M., "Conditional Sampling in a Transitional Boundary Layer Under High Free-Stream Turbulence Conditions," *Journal of Fluids Engineering*, Vol. 125, No. 1, 2003, pp. 28–37.

[8]Lou, w., and Hourmouziadis, J., "Separation Bubbles Under Steady and Periodic-Unsteady Main Flow Conditions," *Journal of Turbomachinery*, Vol. 122, No. 4, 2000, pp. 634–643.

[9]Wolff, S., Brunner, S., and Fottner, L., "The Use of Hot-Wire Anemometry to Investigate Unsteady Wake-Induced Boundary-Layer Development on a High Lift LP Turbine Cascade," *Journal of Turbomachinery*, Vol. 122, No. 4, 2000, pp. 644–650.

[10]Kaszeta, R. W., "Experimental Investigation of Transition to Turbulence as Affected by Passing Wakes," Ph.D. Thesis, Dept. of Mechanical Engineering, Univ. of Minnesota, Minneapolis, MN, May 2000.

[11]Kaszeta, R. W., and Simon, T. W., "Experimental Investigation of Transition to Turbulence as Affected by Passing Wakes," NASA-CR-212104, June 2002.

[12]Kaszeta, R. W., Simon, T. W., and Ashpis, D. P., "Experimental Investigation of Transition to Turbulence as Affected by Passing Wakes," American Society of Mechanical Engineers, ASME Paper 2001-GT-0195, June 2001.

[13]Kaszeta, R. W., Simon, T. W., Jiang, N., and Ottaviani, F., "Influence of Wake Passing Frequency and Elevated Turbulence Intensity on Transition," *Journal of Thermophysics and Heat Transfer* (to be published).

[14]Yaras, M. I., "Measurement of The Effects of Pressure-Gradient History on Separation-Bubble Transition," American Society of Mechanical Engineers, ASME Paper 2001-GT-0193, June 2001.

[15]Howell, R. J., Hodson, H. P., Schulte, V., Heinz-Peter Schiffer, H., Haselbach, F., and Harvey, N. W., "Boundary Layer Development in the BR710 and BR715 LP Turbines—The Implementation of High Lift and Ultra High Lift Concepts," *Journal of Turbomachinery*, Vol. 124, No. 3, 2002, pp. 385–392.

[16]Yuan, K., "Simulation of Wakes: The Development of a Linear Cascade Wake Generator," M.S. Thesis, Dept. of Mechanical Engineering, Univ. of Minnesota, Minneapolis, MN, May 1999.

[17]Kaszeta, R. W., Ottaviani, F., and Simon, T. W., "Experimental Investigation of Transition to Turbulence as Affected by Passing Wakes: Effects of High FSTI and Increased Rod Spacing," NASA-CR.

[18]Qiu, S., "An Experimental Study of Laminar to Turbulent Flow Transition With Temporal and Spatial Acceleration Effects," Ph.D. Dissertation, Dept. of Mechanical Engineering, Univ. of Minnesota, Minneapolis, MN, May 1996.

[19]Qiu, S., and Simon, T. W., "An Experimental Investigation of Transition as Applied to Low Pressure Turbine Suction Surface Flows," American Society of Mechanical Engineers, ASME Paper 97-GT-455, June 1997.

[20]Jiang, N., and Simon, T. W., "Modeling Laminar-to-Turbulent Transition in a Low-Pressure Turbine Flow Which is Unsteady due to Passing Wakes: Part I, Transition Onset," American Society of Mechanical Engineers, ASME Paper GT2003-38787, June 2003.

[21]Jiang, N., and Simon, T. W., "Modeling Laminar-to-Turbulent Transition in a Low-Pressure Turbine Flow Which is Unsteady due to Passing Wakes: Part II Transition Path," American Society of Mechanical Engineers, ASME Paper GT2003-38963, June 2003.

[22]Falco, R. E., and Gendrich, C. P., "The Turbulence Burst Detection Algorithm of Z. Zarić," *Near-Wall Turbulence 1988 Z. Zarić Memorial Conference*, edited by S. J. Kline and N. H. Afgan, Hemisphere, New York, 1990, pp. 911–931.

[23]Walker, G. J., and Solomon, W. J., "Turbulent Intermittency Measurement on an Axial Compressor Blade," *Eleventh Australasian Fluid Mechanics Conference*, edited by M. R. Davis and G. J. Walker, Univ. of Tasmania, Hobart, 1992, pp. 1277–1280.

[24]Bellhouse, B. J., and Schultz, D. L., "Determination of Mean and Dynamic Skin Friction, Separation and Transition in Low-Speed Flow with a Thin-Film Heated Element," *Journal of Fluid Mechanics*, Vol. 24, Pt. 2, 1966, pp. 379–400.

[25]Ottaviani, F., "The Influence of Passing Wake Frequency and Elevated Turbulence on Transition in Low-Pressure Turbines," M.S. Thesis, Dept. of Mechanical Engineering, Univ. of Minnesota, Minneapolis, MN, July 2001.

[26]Emmons, H. W., "The Laminar–Turbulent Transition in a Boundary Layer," *Journal of the Aeronautical Sciences*, Vol. 18, No. 7, July 1951, pp. 490–498.